

TOPICAL REVIEW — ZNO-RELATED MATERIALS AND DEVICES

## ZnO-based deep-ultraviolet light-emitting devices

To cite this article: Ying-Jie Lu *et al* 2017 *Chinese Phys. B* **26** 047703

View the [article online](#) for updates and enhancements.

### Related content

- [Topical Review](#)  
Dae-Kue Hwang, Min-Suk Oh, Jae-Hong Lim *et al*.
- [Optoelectronic device physics and technology of nitride semiconductors from the UV to the terahertz](#)  
Theodore D Moustakas and Roberto Paiella
- [Electrically pumped random lasers](#)  
S F Yu

### Recent citations

- [Diamond-Based All-Carbon Photodetectors for Solar-Blind Imaging](#)  
Chao-Nan Lin *et al*
- [Localized Surface Plasmon Enhanced All-Inorganic Perovskite Quantum Dot Light-Emitting Diodes Based on Coaxial Core/Shell Heterojunction Architecture](#)  
Zhifeng Shi *et al*

## ZnO-based deep-ultraviolet light-emitting devices\*

Ying-Jie Lu(卢英杰)<sup>1</sup>, Zhi-Feng Shi(史志锋)<sup>1</sup>, Chong-Xin Shan(单崇新)<sup>1,2,†</sup>, and De-Zhen Shen(申德振)<sup>2</sup><sup>1</sup>School of Physics and Engineering, Zhengzhou University, Zhengzhou 450001, China<sup>2</sup>State Key Laboratory of Luminescence and Applications, Changchun Institute of Optics, Fine Mechanics and Physics, Chinese Academy of Sciences, Changchun 130033, China

(Received 22 October 2016; revised manuscript received 27 November 2016; published online 10 March 2017)

Deep-ultraviolet (DUV) light-emitting devices (LEDs) have a variety of potential applications. Zinc-oxide-based materials, which have wide bandgap and large exciton binding energy, have potential applications in high-performance DUV LEDs. To realize such optoelectronic devices, the modulation of the bandgap is required. This has been demonstrated by the developments of  $\text{Mg}_x\text{Zn}_{1-x}\text{O}$  and  $\text{Be}_x\text{Zn}_{1-x}\text{O}$  alloys for the larger bandgap materials. Many efforts have been made to obtain DUV LEDs, and promising successes have been achieved continuously. In this article, we review the recent progress of and problems encountered in the research of ZnO-based DUV LEDs.

**Keywords:** ZnO, deep-ultraviolet light-emitting devices,  $\text{Mg}_x\text{Zn}_{1-x}\text{O}$ ,  $\text{Be}_x\text{Zn}_{1-x}\text{O}$ **PACS:** 77.55.hf, 78.45.+h, 78.60.Fi, 85.60.Jb**DOI:** 10.1088/1674-1056/26/4/047703

## 1. Introduction

Deep-ultraviolet (DUV) light-emitting devices (LEDs) with wavelengths shorter than 300 nm have a variety of potential applications in several areas, such as air, water and surface sterilization, medical diagnosis and therapy, radiation hard UV sources, UV curing, etc.<sup>[1–3]</sup> With the increasing awareness of health risks caused by contaminated food, air, and water, demands for purification products based on compact and cost-effective semiconductor UV sources are expanding. Nevertheless, currently the most frequently used DUV light source (i.e., mercury lamp) is usually bulky and costly, even worse, it brings the risk of the possible heavy metal pollution, all of which hinder such DUV light source from being used in many areas. As a promising alternative to mercury lamp, the wide bandgap semiconductor based DUV light source has a variety of figure-of-merits such as low-power consumption, high-efficiency, compact size, long lifetime, low pollution, etc., thus much attention has been paid to this area in recent years.<sup>[4–10]</sup> For a DUV LED, the bandgap of the active semiconductor layer should be larger than 4.1 eV. On one hand, the wide bandgap semiconductors such as diamond and BN are suitable active layers for DUV LEDs.<sup>[11,12]</sup> On the other hand, the group-III nitride and group-II oxide semiconductors whose bandgaps can be tuned to DUV range are very useful for UV and DUV optoelectronic device applications.<sup>[13–15]</sup> Zinc oxide (ZnO) has a large exciton binding energy of 60 meV and a wide bandgap of 3.37 eV at room-temperature (RT), which may realize exciton luminous, and has potential applications in the areas of high-performance

UV LEDs and laser diodes.<sup>[16–18]</sup> Moreover, the band gap of ZnO can be modulated to realize the DUV LEDs. This has been demonstrated by the developments of  $\text{Mg}_x\text{Zn}_{1-x}\text{O}$  and  $\text{Be}_x\text{Zn}_{1-x}\text{O}$  ternary alloys for the larger bandgap active layers.<sup>[19–24]</sup> Many efforts have been made to develop ZnO-based DUV LEDs, and some results have been obtained. In this paper, we will briefly review the recent research progress of ZnO-based DUV LEDs based on p–n heterostructures and metal-insulator-semiconductor (MIS) heterostructures.

## 2. DUV LEDs with MgZnO as the active layer

The bandgap of MgO is approximately 7.8 eV, and the bandgap of ZnO is about 3.37 eV. Therefore, the bandgap of MgZnO alloy can be tuned in a large range from 3.3 eV to 7.8 eV. So by alloying with MgO, ZnO can be extended to the DUV region. In addition, the exciton binding energy ( $E_B$ ) of cubic MgO ( $E_B \sim 80$  meV) is also larger than that of wurtzite ZnO (60 meV),<sup>[25]</sup> which might be advantageous for DUV excitonic light emitter applications. Moreover, compared with other wide bandgap semiconductors, MgZnO has some unique features, such as the high resistance to radiation, the amenability to conventional wet chemistry etching, the environment-friendly characteristics, and the relatively low growth temperatures, which make MgZnO alloy a promising candidate as the DUV light-emitter. To realize high-performance semiconductor LED, p–n junction should be constructed in general. So high-quality n- and p-type MgZnO are both indispensable. While ZnO is intrinsically of n-type conduction, that is, n-type MgZnO can be relatively easy to obtain. However, p-type dop-

\*Project supported by the National Natural Science Foundation for Distinguished Young Scholars of China (Grant No. 61425021) and the Natural Natural Science Foundation of China (Grant Nos. 11374296, 61376054, 61475153, and 61604132).

†Corresponding author. E-mail: shanx@ciomp.ac.cn

ing of ZnO is still an obstacle. Considering its wider bandgap, the p-type doping of MgZnO may be more challenging due to the relatively large activation energy of acceptors.<sup>[26–28]</sup>

## 2.1. p-MgZnO-based heterojunction DUV LEDs

To obtain p-type MgZnO, the lithium and nitrogen codoping method was developed by using plasma-assisted molecular beam epitaxy technique, and the p-type conduction

of MgZnO films were also obtained.<sup>[29–31]</sup> Typically, the hole concentration and mobility were about  $10^{16} \text{ cm}^{-3}$  and  $1 \text{ cm}^2/\text{Vs}$ , respectively. The reproducible p-type doping of MgZnO has been proved to be a feasible route.<sup>[29–31]</sup> To test the applicability of the p-MgZnO film in optoelectronic device, p-MgZnO:(Li:N)/i-ZnO/n-ZnO structure LEDs have been constructed,<sup>[29]</sup> and the schematic diagram of the LED is shown in the inset of Fig. 1(a).

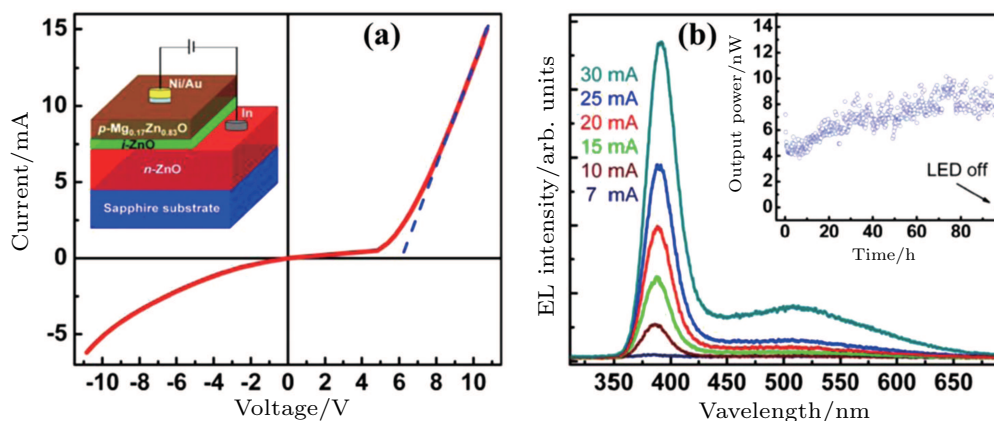


**Fig. 1.** (color online)  $I$ - $V$  curve of the p-MgZnO:(Li:N)/i-ZnO/n-ZnO structure. The inset shows a schematic illustration of the structure. (b) The room temperature (RT) electroluminescence (EL) spectra of the structure under different injection currents. The inset shows the output power of the LED as a function of its running time with an injection current of 20 mA. Note that the last scatter symbol indicates the emission intensity when the LED is switched off.<sup>[29]</sup>

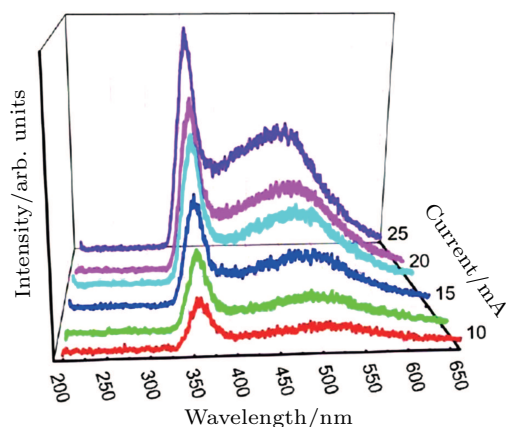


**Fig. 2.** (color online) RT EL spectra of the p-Mg<sub>0.35</sub>Zn<sub>0.65</sub>O:(Li:N)/n-Mg<sub>0.20</sub>Zn<sub>0.80</sub>O heterostructure at different injection currents.<sup>[29]</sup>

The current-voltage ( $I$ - $V$ ) characteristics of the p-MgZnO:(Li:N)/i-ZnO/n-ZnO heterostructured LEDs are illustrated in Fig. 1(a), and typical rectification behavior was observed with a turn-on voltage of about 6.0 V. The electroluminescence (EL) spectra of the device are shown in Fig. 1(b). By employing i-ZnO film as an active layer, the spectra show a dominant emission at around 390 nm, which comes from the near-band-edge (NBE) emission of ZnO. To shorten the emission wavelength of the heterostructured LED, wider bandgap MgZnO film must be employed as the active layer. Then Liu *et al.* further constructed p-Mg<sub>0.35</sub>Zn<sub>0.65</sub>O/n-Mg<sub>0.20</sub>Zn<sub>0.80</sub>O heterostructured LEDs. The room-temperature EL spectra of the heterostructure at various injection currents are shown in Fig. 2. A dominant UV emission peaked at around 355 nm

has been observed from the heterostructures.<sup>[32]</sup> Compared with the former one, the emission wavelength of this device is shortened obviously, but it is still not up to the DUV region. To obtain the DUV emission, the bandgap of MgZnO must be further adjusted, and the corresponding mole percentage of  $\text{Mg}^{2+}$  in MgZnO must be increased further. However, the efficient p-type doping of such a large bandgap material becomes almost impossible. In this circumstance, it was suggested that the desired DUV emission from MgZnO film should be obtained by using other methods.

## 2.2. n-MgZnO-based heterojunction DUV LEDs

In order to bypass the challenging p-type doping of wide bandgap MgZnO, the MgZnO-based heterostructures have been extensively studied by employing p-GaN as the hole-transporting layer recently.<sup>[15,33–35]</sup> In 2009, Zhu *et al.* reported on the fabrication of an n-Mg<sub>0.12</sub>Zn<sub>0.88</sub>O/p-GaN heterojunction LED with an MgO dielectric interlayer by plasma-assisted molecular beam epitaxy technique.<sup>[34]</sup> By the proper engineering of the band alignment of the heterojunction with using the MgO layer, most electrons are confined in the Mg<sub>0.12</sub>Zn<sub>0.88</sub>O layer under positive bias, while holes can be injected into the Mg<sub>0.12</sub>Zn<sub>0.88</sub>O active layer from the p-GaN side, and the typical EL spectra from the heterostructure are shown in Fig. 3. Under forward bias, an UV emission located at around 374-nm coming from the Mg<sub>0.12</sub>Zn<sub>0.88</sub>O films is observed. The right inset of Fig. 3 displays a colored photograph

taken from the device at 11.5 mA.

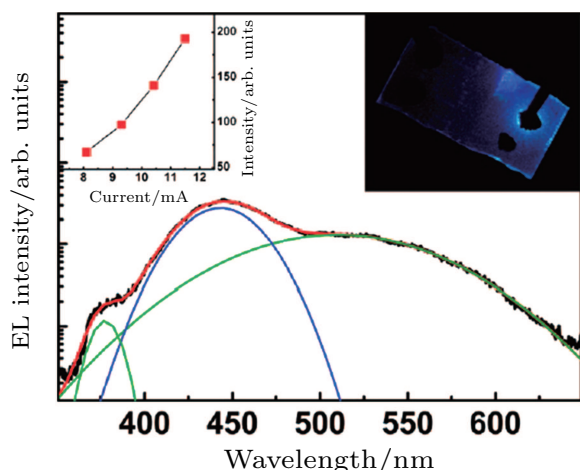


**Fig. 3.** (color online) EL spectra of the n-Mg<sub>0.12</sub>Zn<sub>0.88</sub>O/MgO/p-GaN heterostructured device with an injection current of 11.5 mA. The two insets show the EL intensity of the 374-nm peak versus the injection current and a typical emission photograph of the device, respectively.<sup>[34]</sup> Reprinted with permission from (Ultraviolet Electroluminescence from MgZnO-Based Heterojunction Light-Emitting Diodes). Copyright (2009) American Chemical Society.

In 2011, Chu *et al.* demonstrated the growth of high-quality MgZnO nanowires on p-GaN films by chemical vapor deposition method,<sup>[35]</sup> and further fabricated an n-MgZnO/p-GaN heterojunction LED for DUV emission applications, in which the atomic ratio of Zn-to-Mg is 84:16 as determined by the energy-dispersive x-ray spectroscopy. In order to separate the metal contact on the top of the Mg<sub>0.16</sub>Zn<sub>0.84</sub>O nanowires from the substrate, a layer of poly(methylmethacrylate) (PMMA) was spun onto the sample, leaving the tip of some wires uncovered. A UV emission at 340 nm can be detected under forward bias, corresponding to the radiative recombination in Mg<sub>0.16</sub>Zn<sub>0.84</sub>O nanowires. However, this n-Mg<sub>0.16</sub>Zn<sub>0.84</sub>O/p-GaN heterojunction LED suffers a poor emission purity because other two emission peaks at 363 nm and 392 nm also emerge, and the corresponding emission intensities also increase with injection current increasing. The above observations suggest that the Mg<sub>0.16</sub>Zn<sub>0.84</sub>O active layer does not serve as the sole recombination zone in the n-Mg<sub>0.16</sub>Zn<sub>0.84</sub>O/p-GaN heterojunction. From the device point of view, the charge carrier transport behavior must be optimized further under the premise of a high-quality MgZnO active layer with a high Mg content. Thus, MgZnO-based heterostructures may find future applications in DUV optoelectronics.

### 2.3. MIS heterojunction DUV LEDs

Another alternative route to DUV LEDs from wide bandgap semiconductors is the MIS heterostructure. This route could avoid the obstacle of p-type doping of wide bandgap semiconductors, and it has been confirmed to be feasible.<sup>[36–39]</sup> In the early stage of the development of ZnO-

based LEDs, MIS heterostructure by using high-resistance intrinsic ZnO (i-ZnO) as the insulator layer was an important candidate.<sup>[40–42]</sup> However, the EL spectra obtained from MIS heterostructure are often characterized by a dominant deep-level visible emission, and the band-to-band transition corresponding to the UV emission is not the main contributor. In the last few years, another kind of ZnO-based MIS heterostructure obtained by using insulating materials (MgO, SiO<sub>2</sub>, AlN, etc.) with relatively larger bandgap as the insulator layer has become popular and attracted increasingly attention. In 2006, Chen *et al.* reported their research on Au/SiO<sub>2</sub>/ZnO MIS LEDs, and realized a fairly UV emission under a continuous current injection.<sup>[43]</sup> In 2010, Zhu *et al.* demonstrated the electrically pumped UV random lasing from ZnO nanocrystalline films based on Au/MgO/ZnO MIS heterostructures,<sup>[44]</sup> and showed the corresponding schematic illustration of the device in Fig. 4(a). Its carrier transport behavior and EL mechanism can be simply described as follows. As shown in Fig. 4(b), the conduction and valence band offsets ( $\Delta E_C$ ,  $\Delta E_V$ ) at the MgO/ZnO interface can be determined to be 3.55 eV and 0.88 eV, respectively. Under a forward bias, electrons would be blocked and available in abundance at the MgO/ZnO interface because of the existence of high  $\Delta E_C$ . And meanwhile, a sufficiently high bias enables the holes to be generated in the MgO layer due to the high-electric-field-induced impact ionization process, with considering the fact that almost all the voltage is applied to the insulating layer and the local electrical field strength could be as high as  $\sim 10^6$  V/m therein. Above a critical driving voltage, the generated holes can be swept into the valence band of ZnO, and recombine radiatively with the electrons accumulated at the MgO/ZnO interface, producing the NBE emission and even UV lasing.

It seems easy to construct an Au/MgO/MgZnO structure to obtain UV LED with a shorter emission wavelength. However, the electron concentration in MgZnO film decreases dramatically with the increase of Mg component, which will restrict the concentration of non-equilibrium carriers in the active layer and also the luminous efficiency. To solve this problem, an electron providing layer is introduced to enhance the electron injection into the MgZnO active layer and an Au/MgO/MgZnO/n-ZnO heterostructure is therefore constructed.<sup>[45]</sup> The corresponding schematic illustration of the Au/MgO/MgZnO/n-ZnO structure is shown in Fig. 5(a). More importantly, electrically pumped UV lasing has been realized in this heterostructure with the lasing peak at around 330 nm (shown in Fig. 5(b)), and the dependence of the integrated EL intensity as a function of injection current reveals a lasing threshold of 30 mA. Although the emission obtained in the device is not in the DUV spectral range, this is one of the shortest wavelengths ever reported in a semiconductor laser diode.

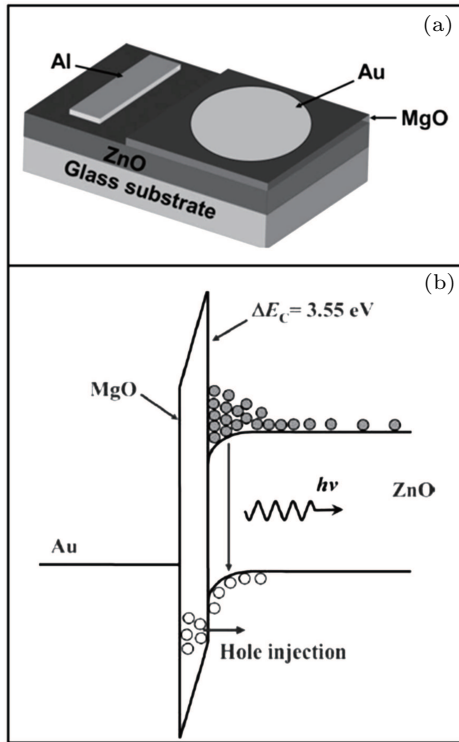


**Fig. 4.** (color online) (a) Schematic illustration of the Au/MgO/ZnO structure. (b) Band alignment of the Au/MgO/ZnO structure under forward bias, showing the generation, multiplication, and injection of electrons and holes.<sup>[44]</sup> Reproduced from Ref. [45] with permission from the Royal Society of Chemistry.

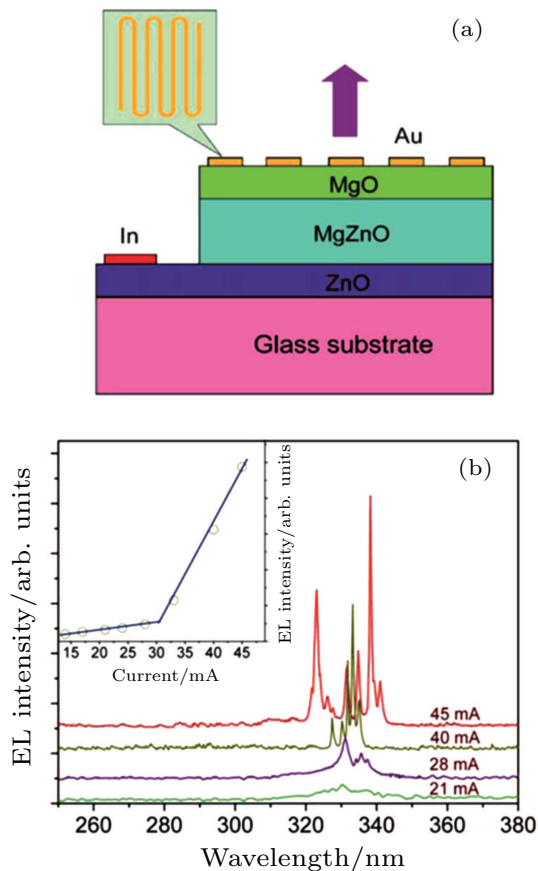


**Fig. 5.** (color online) (a) The schematic illustration of the Au/MgO/MgZnO/n-ZnO structure. (b) Lasing spectra of the device under different injection currents. The inset shows the integrated intensity of the emission at around 330 nm as a function of the injection current.<sup>[45]</sup>

Although the n-ZnO layer with a high electron concentration can serve as an electron injector, the large  $\Delta E_C$  between ZnO and MgZnO forms a large energy barrier which hinders the electrons from being injected from n-ZnO to MgZnO active layer. With increasing the bandgap of MgZnO active layer, the barrier becomes large accordingly. To solve this problem, a composition-gradient  $\text{Mg}_x\text{Zn}_{1-x}\text{O}$  layer has been employed to build a bridge between the MgZnO active layer and n-ZnO electron source layer to assist the electrons to drift from ZnO to MgZnO layer. According to this idea, Zhu *et al.* fabricated an Au/MgO/Mg<sub>0.52</sub>Zn<sub>0.48</sub>O/Mg<sub>x</sub>Zn<sub>1-x</sub>O/n-ZnO structure,<sup>[46]</sup> and showed the schematic structure of this device in the inset of Fig. 6(a). In this structure, the thickness of Mg<sub>x</sub>Zn<sub>1-x</sub>O layer was about 100 nm, with  $x$  changing from 0 to 0.52 gradually. The  $I$ - $V$  characteristic of the device exhibits an obvious rectification characteristic with a turn-on voltage of about 26.0 V. The corresponding band alignment of the Au/MgO/Mg<sub>0.52</sub>Zn<sub>0.48</sub>O/Mg<sub>x</sub>Zn<sub>1-x</sub>O/n-ZnO structure is shown in Fig. 6(b). Owing to the assistance of a composition-gradient Mg<sub>x</sub>Zn<sub>1-x</sub>O bridging layer, the injection process of electrons from n-ZnO to Mg<sub>0.52</sub>Zn<sub>0.48</sub>O active layer will be facilitated.

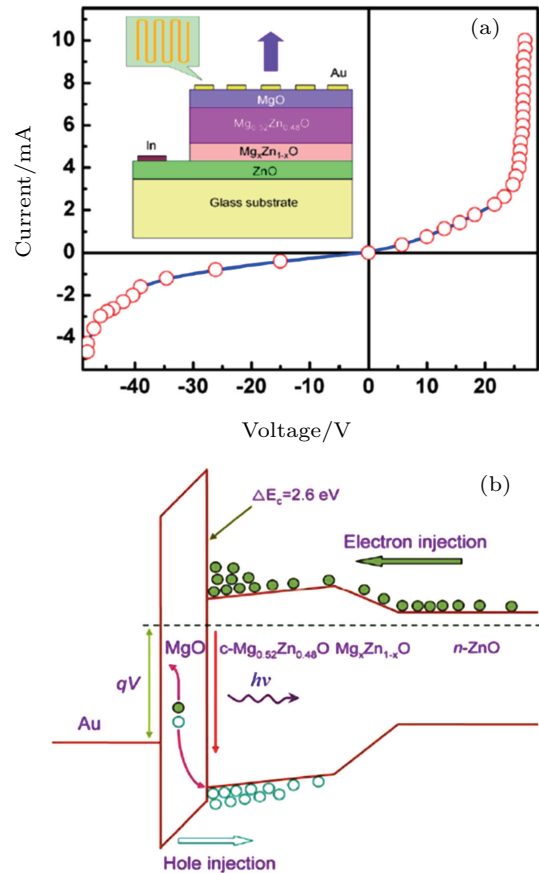


**Fig. 6.** (color online) (a) The typical  $I$ - $V$  curve of the Au/MgO/Mg<sub>0.52</sub>Zn<sub>0.48</sub>O/Mg<sub>x</sub>Zn<sub>1-x</sub>O/n-ZnO structure, and the inset shows a schematic illustration of the structure. (b) Bandgap diagram of the structure under forward bias, showing the generation, multiplication, and injection of electrons and holes.<sup>[46]</sup>



One can see that the bandgap of the  $\text{Mg}_x\text{Zn}_{1-x}\text{O}$  layer is enlarged with the increase of Mg content. As a result, the energy barrier between ZnO and  $\text{Mg}_{0.52}\text{Zn}_{0.48}\text{O}$  increases gradually rather than suddenly, so the electrons may be easier to inject. The EL spectra of the device are shown in Fig. 7. At a low forward bias, few electrons can be injected into the  $\text{Mg}_{0.52}\text{Zn}_{0.48}\text{O}$  and MgZnO layers, and the holes generated in the MgO layer via impact ionization can drift to the  $\text{Mg}_{0.52}\text{Zn}_{0.48}\text{O}$  and MgZnO, or even the n-ZnO layer, recombining with electrons in these layers. Therefore, weak emissions from the  $\text{Mg}_{0.52}\text{Zn}_{0.48}\text{O}$ , MgZnO, and n-ZnO layers have been observed as indicated by the EL spectra with the driving currents of 30 mA and 40 mA. Further increasing the current to a higher value of 50 mA, the strong accumulation and confinement of the injected electrons adjacent to the  $\text{MgO}/\text{Mg}_{0.52}\text{Zn}_{0.48}\text{O}$  interface are ensured, thus an obvious DUV emission at around 276 nm was detected, corresponding to the NBE emission from  $\text{Mg}_{0.52}\text{Zn}_{0.48}\text{O}$  layer. The inset shows the dependence of the output power of the device on the injection current. The output power of the device is on the order of nanowatt and it increases with the injection current increasing. It is anticipated that the results will provide a promising route to high-performance DUV LEDs based on the hole-multiplication process by passing the problematic p-type doping method.

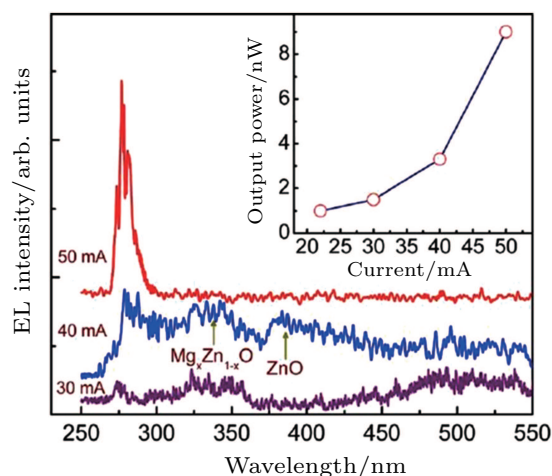


**Fig. 7.** (color online) The electroluminescence spectra of the  $\text{Au}/\text{MgO}/\text{Mg}_{0.52}\text{Zn}_{0.48}\text{O}/\text{Mg}_x\text{Zn}_{1-x}\text{O}/\text{n-ZnO}$  structure under the injection of continuous current at RT, and the inset shows the dependence of output power on the injection current.<sup>[46]</sup>

The introducing of the impact ionization process to produce holes could avoid the dependence on p-type doping of MgZnO, but the holes produced by this route are inefficient. More importantly, such devices are generally operated under high voltages, so the undesired heating effect is very serious. Thus the prospect of this structure is definitely bleak. Another method to realize DUV emissions of wide bandgap semiconductor is to use the electron beam as an excitation source.<sup>[3]</sup> It can be accepted that the accelerated energetic

electrons can excite the electrons in the valence band of semiconductors into its conduction band, giving rise to free electrons and holes. The electrons in the conduction band will recombine with the generated holes in the valence band, as a result, emissions will be realized. By employing this method, the UV emissions were demonstrated.<sup>[1,2,47,48]</sup> Traditionally, the high-energy electron-beam was generated in a vacuum atmosphere at high voltage, which makes the facility bulky and costly. Fortunately, some reports on visible emissions excited by electron-beams in solid-state structure have been demonstrated.<sup>[49–52]</sup>

In terms of UV emission, Ni *et al.* constructed  $\text{Au}/\text{i-ZnO}/\text{n-ZnO}$  structure,<sup>[53]</sup> in which the i-ZnO serves as an electron accelerating layer, and n-type ZnO acts as an active layer. The UV emission at around 385 nm has been realized, which is caused by the excitation of the n-ZnO layer by the accelerated electrons from the i-ZnO. For shorter wavelength emissions, an  $\text{Au}/\text{Mg}_{0.39}\text{Zn}_{0.61}\text{O}/\text{MgO}/\text{n-ZnO}$  structure has been designed and fabricated, and the schematic diagram of this structure is shown in Fig. 8(a). In this structure, the n-ZnO film acts as an electron source, the MgO layer is an electron-accelerating layer, and the  $\text{Mg}_{0.39}\text{Zn}_{0.61}\text{O}$  films work as the active layer. As shown in the band diagram of this structure in Fig. 8(b), under the reverse bias (the negative voltage was applied on n-ZnO) the electrons in the n-ZnO layer will be concentrated at the  $\text{MgO}/\text{ZnO}$  interface due to the large  $\Delta E_C$  (3.55 eV) between the MgO and ZnO. Considering that most of the bias will be applied to the MgO layer due to its dielectric nature, the conduction and valence bands of the MgO layer will bend drastically. Then the width of the barrier that hinders the electrons in the n-ZnO from tunneling to the  $\text{Mg}_{0.39}\text{Zn}_{0.61}\text{O}$  layer will be greatly reduced. As a result, many electrons can tunnel through the MgO layer and be injected into the  $\text{Mg}_{0.39}\text{Zn}_{0.61}\text{O}$  active layer. Note that when the electrons enter into the MgO layer, they will be accelerated greatly due to the large electric field in this layer. Then the accelerated electrons will release their energy by generating free electrons and holes in the MgZnO layer. When these generated holes recombine with the free electrons, band-to-band emissions will be achieved.

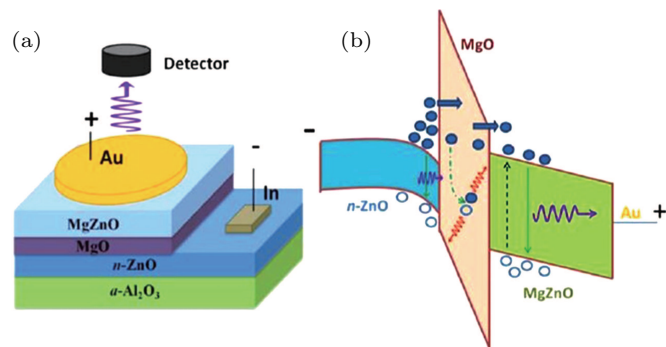


**Fig. 8.** (color online) (a) Schematic diagram of the  $\text{Mg}_{0.39}\text{Zn}_{0.61}\text{O}/\text{MgO}/\text{n-ZnO}$  structure. (b) Band diagram of the  $\text{MgZnO}/\text{MgO}/\text{n-ZnO}$  structure under reverse bias.<sup>[53]</sup>

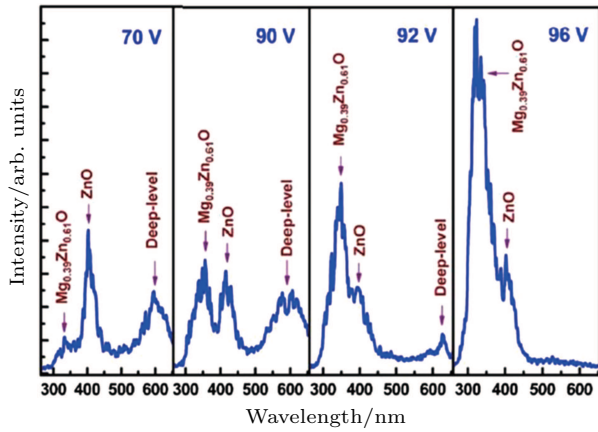


Fig. 9. (color online) Emission spectra of Au/Mg<sub>0.39</sub>Zn<sub>0.61</sub>O/MgO/n-ZnO structure under different reverse biases.<sup>[53]</sup>

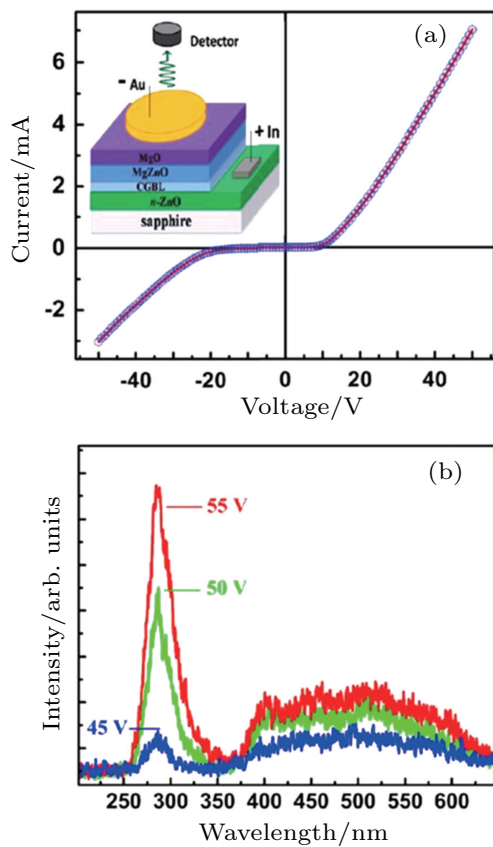


Fig. 10. (color online) (a) The  $I$ - $V$  characteristic of the Au/MgO/Mg<sub>0.51</sub>Zn<sub>0.49</sub>O/Mg<sub>x</sub>Zn<sub>1-x</sub>O/n-ZnO structure, and the inset shows the schematic diagram and emission recording geometry of the structure. (b) Emission spectra of the structure under different reverse bias voltages.<sup>[54]</sup>

The emission spectra of the structure under different reverse biases are shown in Fig. 9. An obvious ultraviolet emission at around 328 nm has been obtained. And an additional observation is that the band-to-band transition (328 nm) from Mg<sub>0.39</sub>Zn<sub>0.61</sub>O active layer dominates over the NBE and defect-related transitions from ZnO with the increase of driving current. By replacing the active layer with a larger bandgap Mg<sub>0.51</sub>Zn<sub>0.49</sub>O and properly optimizing the device structure, DUV emission at around 285 nm has been obtained.<sup>[54]</sup> The  $I$ - $V$  characteristic of the

constructed Au/MgO/Mg<sub>0.51</sub>Zn<sub>0.49</sub>O/Mg<sub>x</sub>Zn<sub>1-x</sub>O/n-ZnO heterostructure is shown in Fig. 10(a), and the inset shows the corresponding schematic diagram of the structure. The detected emission spectra of the structure under different reverse bias voltages are illustrated in Fig. 10(b).

### 3. DUV LEDs with BeMgZnO as active layer

Due to the different crystal structures and large lattice mismatch between ZnO (3.25 Å, hexagonal) and MgO (4.22 Å, cubic), the phase separation or precipitation will occur when the Mg concentration is above a certain limit that is dependent on the film deposition process.<sup>[55–57]</sup> Generally, the phase segregation was observed from the Mg<sub>x</sub>Zn<sub>1-x</sub>O alloy with more than 36% of Mg atomic content and the bandgap of the alloy is usually limited to a value less than 4.0 eV.<sup>[58]</sup> So the MgZnO material is not very efficient for developing deeper UV LEDs to some extent. In these circumstances, hexagonal Be<sub>x</sub>Zn<sub>1-x</sub>O materials attract our intensive attention. It is because that BeO and ZnO share the same hexagonal wurtzite structure, and BeO has a good solubility with ZnO, so the atomic ratio of Be-to-Zn in Be<sub>x</sub>Zn<sub>1-x</sub>O film can be any value.<sup>[59]</sup> More importantly, the produced Be<sub>x</sub>Zn<sub>1-x</sub>O film is wurtzitic throughout the entire compositional range without the phase segregation phenomenon occurring. It has been reported that the bandgap of Be<sub>x</sub>Zn<sub>1-x</sub>O ( $0 \leq x \leq 1$ ) films can be adjusted from 3.37 ( $x = 0$ ) to 10.6 eV ( $x = 1$ ),<sup>[60]</sup> and the energy bandgaps of Be<sub>x</sub>Zn<sub>1-x</sub>O as a function of Be content are plotted in Fig. 11.

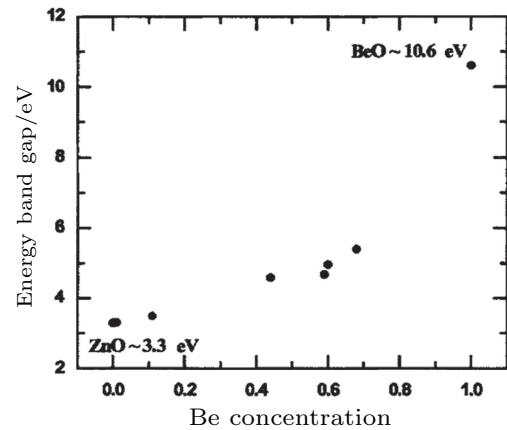
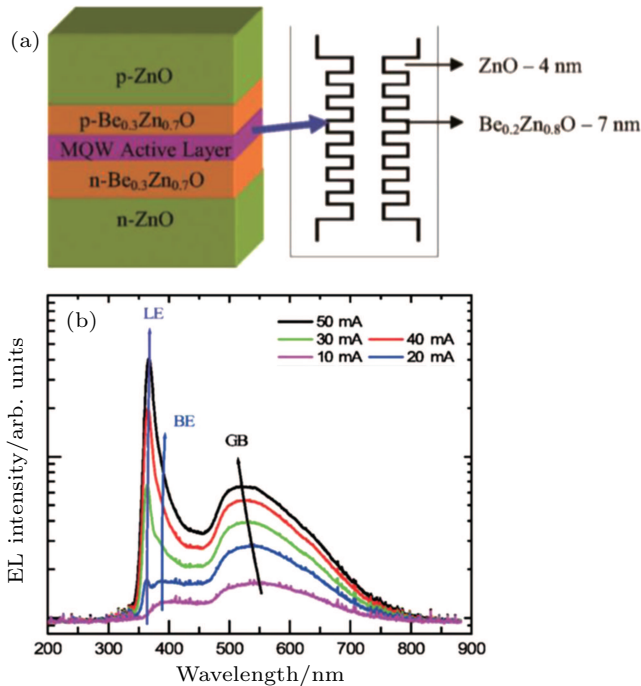


Fig. 11. (color online) Energy band gaps of BeZnO as a function of Be concentration in atomic fraction.<sup>[60]</sup>

In 2006, Ryu *et al.* reported ZnO-based UV LED where a BeZnO/ZnO active layer between n-type and p-type ZnO and the Be<sub>0.3</sub>Zn<sub>0.7</sub>O layer were used.<sup>[61]</sup> The active layer is composed of seven quantum wells in which undoped Be<sub>0.2</sub>Zn<sub>0.8</sub>O and ZnO serve as barrier and well layers, respectively. The p-ZnO and p-Be<sub>0.3</sub>Zn<sub>0.7</sub>O layers are realized with arsenic used as the acceptor dopant, while n-ZnO and n-Be<sub>0.3</sub>Zn<sub>0.7</sub>O layers were realized with gallium used as the dopant. The schematic illustration of the device structure is shown in Fig. 12(a),

and the detected EL spectra at different injection currents are shown in Fig. 12(b). At a low driving current of 10 mA, the emission peaks at 388 nm and 550 nm dominate the EL spectra. The former can be ascribed to the impurity-bound exciton emission, and the latter may come from the donor-acceptor pair recombination. With the increase of the injection current, a new emission peak at 363 nm emerges and becomes dominant at higher current levels. By comparing with the photoluminescence spectra of the  $\text{Be}_{0.2}\text{Zn}_{0.8}\text{O}/\text{ZnO}$  superlattices, the authors attributed the emission peak at 363 nm to the localized-exciton recombination in the  $\text{Be}_{0.2}\text{Zn}_{0.8}\text{O}/\text{ZnO}$  quantum wells.



**Fig. 12.** (color online) (a) Schematic illustration of the ZnO-based LED where a  $\text{BeZnO}/\text{ZnO}$  active layer comprised of multiple quantum wells is used. (b) EL spectra of the diode measured at RT in a continuous current mode.<sup>[61]</sup>

After that, Ryu *et al.* reported the excitonic stimulated emission and lasing generated by electrical pumping from  $\text{BeZnO}/\text{ZnO}$ -based devices,<sup>[62]</sup> and the devices were fabricated by using the same growth and fabrication methods as that we introduced above. The device structure is based on a p-n heterojunction with a multiple quantum well active layer sandwiched between guide-confinement layers. The multiple quantum well active layer is comprised of undoped ZnO and  $\text{BeZnO}$ , while the two guide-confinement layers were As-doped p-type  $\text{ZnO}/\text{BeZnO}$  and Ga-doped n-type  $\text{BeZnO}/\text{ZnO}$  films, respectively. Figure 13 shows the detected EL spectra measured at RT in pulsed mode (10% duty cycle) current injection. As the current increases, the sharp Fabry-Pérot type oscillations at around 3.21 eV became more prominent, indicating the realization of UV lasing action with a threshold current density of  $420 \text{ A/cm}^2$ . In this case, a large exciton binding energy ( $\sim 263 \text{ meV}$ ) in  $\text{BeZnO}/\text{ZnO}$  quantum well should

be responsible for the exciton-related lasing action realized at room temperature.

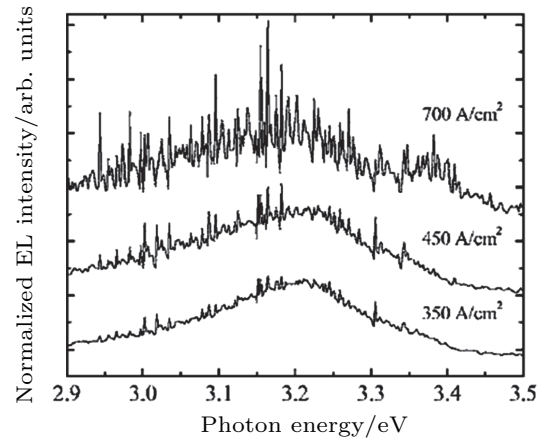


**Fig. 13.** EL spectra measured at RT in pulse current injection mode (10% duty cycle).<sup>[62]</sup>

In order to improve the device performance of  $\text{BeZnO}$ -based UV LED further, two-dimensional numerical simulation was employed to assess a number of possible design approaches aiming at optimizing the internal quantum efficiency (IQE) of  $\text{BeZnO}$ -based LED grown along the  $c$  axis.<sup>[63]</sup> For a high-efficiency operation at a wavelength of 360 nm, the effects of thickness, doping, and alloy composition of  $\text{BeZnO}$  electron blocking layer (EBL) in this heterostructure were in detail analyzed to maximize the carrier confinement in the action region. They found that if the EBL is thicker than 10 nm and has a Be molar fraction in excess of 11%; it can operate effectively as long as the doping is of p-type and at least equal to  $5 \times 10^{18} \text{ cm}^{-3}$  in concentration. And they also found that the optimum number of quantum wells in the active region is three for current densities between  $1 \text{ A/mm}^2$  and  $2 \text{ A/mm}^2$ , while for higher current densities five quantum wells should be employed. Even so, the authors recognized that the  $\text{BeZnO}$  alloy is a relatively immature material at present for UV LEDs with shorter wavelength and higher efficiency, and significant developments in doping techniques and improvement in carrier mobility have to be achieved.

Lately, Chen *et al.* demonstrated the feasibility of Be to enhance N doping concentration in ZnO, and a small amount of Be (less than 1%) in  $\text{BeZnO}$  alloy can greatly increase the concentration of N by more than one order.<sup>[64]</sup> The typical hole concentration and mobility of  $\text{BeZnO:N}$  are  $4.1 \times 10^{16} \text{ cm}^{-3}$  and  $0.2 \text{ cm}^2/\text{V}\cdot\text{s}$ , respectively. Based on the reliable p-type  $\text{BeZnO:N}$ , UV LED with a p- $\text{BeZnO:N}/\text{i-ZnO}/\text{n-ZnO:Ga}$  structure was constructed and the corresponding schematic diagram is shown in Fig. 14(a). The resulting p-i-n junction exhibits excellent diode characteristics, and strong NBE emission at around 390 nm dominates in the spectra as shown in Fig. 14(b), which can be attributed to the donor-acceptor pair transition in p- $\text{BeZnO:N}$  film. The insets show the dependence of the integrated emission intensity on



the injection current and the optical images of the device with different drive currents.

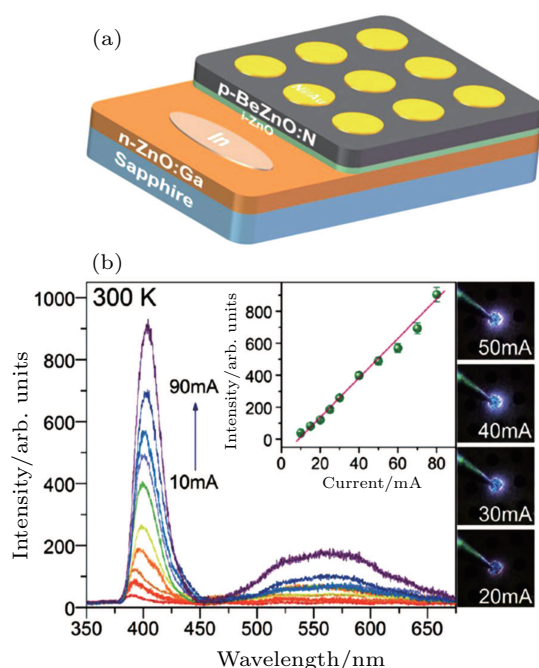


**Fig. 14.** (color online) (a) Schematic diagram of the ZnO p-i-n structure. (b) The EL spectra and the optical images of the ZnO LED under different injection currents at 300 K, the insets indicate how the integrated NBE emission intensity is dependent on the injection current.<sup>[64]</sup>

Although  $\text{Be}_x\text{Zn}_{1-x}\text{O}$  alloys each have a larger bandgap modulation range than the  $\text{Mg}_x\text{Zn}_{1-x}\text{O}$  alloys without phase segregation, there are still problems caused by the difference in ionic radius between  $\text{Be}^{2+}$  (0.27 Å) and  $\text{Zn}^{2+}$  (0.60 Å), inducing a large lattice mismatch between BeO and ZnO.<sup>[65]</sup> The crystal quality of the resulting  $\text{Be}_x\text{Zn}_{1-x}\text{O}$  films will be degraded with the increase of Be atomic content. To obtain high-quality ZnO-based films with bandgap modulation to DUV region, quaternary  $\text{Be}_x\text{Mg}_y\text{Zn}_{1-x-y}\text{O}$  alloys were proposed and investigated for applications in various optoelectronic devices.<sup>[66–68]</sup> Figure 15 shows the x-ray diffraction patterns of the BeZnO and the BeMgZnO films with the same bandgap value of 4.5 eV.<sup>[69]</sup> Each of the BeZnO and BeMgZnO films has a wurtzite structure. Compared with the BeZnO films, the BeMgZnO films have much low full-width half maximum values. It suggests that the BeMgZnO has higher crystal quality than BeZnO.

As stated above, the excellent wavelength adjustabilities of  $\text{Be}_x\text{Mg}_y\text{Zn}_{1-x-y}\text{O}$  alloys each with a high crystallinity suggest their applications in UV optoelectronic devices. In 2013, Lee *et al.* prepared the intrinsic BeMgZnO films by using triple targets of MgO, Be, and Zn in a magnetron co-sputtering system.<sup>[70]</sup> The  $\text{i-Be}_{0.083}\text{Mg}_{0.047}\text{Zn}_{0.87}\text{O}$  film displays a optical transmittance higher than 90% at a range of 400 nm–800 nm, and the corresponding optical energy bandgap is about 3.51 eV. Further, the  $\text{i-Be}_{0.083}\text{Mg}_{0.047}\text{Zn}_{0.87}\text{O}$  film was used as the active layer to construct the  $\text{n-MgZnO:Al/i-Be}_{0.083}\text{Mg}_{0.047}\text{Zn}_{0.87}\text{O/p-GaN}$  heterostructure LED, and its

corresponding schematic configuration is shown in Fig. 16(a). The EL spectra detected at RT for the studied diode are shown in Fig. 16(b), with the injection current ranging from 5 mA to 80 mA. One can see that the emission peak from the  $\text{n-MgZnO:Al/i-Be}_{0.083}\text{Mg}_{0.047}\text{Zn}_{0.87}\text{O/p-GaN}$  heterostructured diode is at around 355 nm.

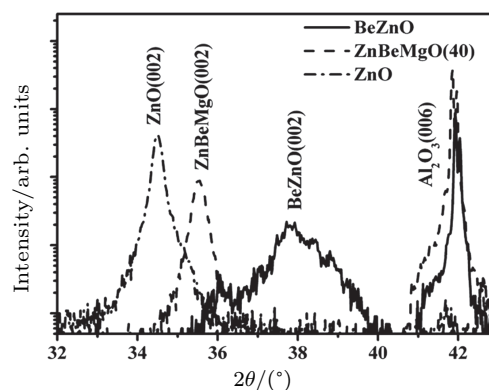


**Fig. 15.** XRD patterns of BeZnO and ZnBeMgO with the same bandgap value of 4.5 eV.<sup>[68]</sup>

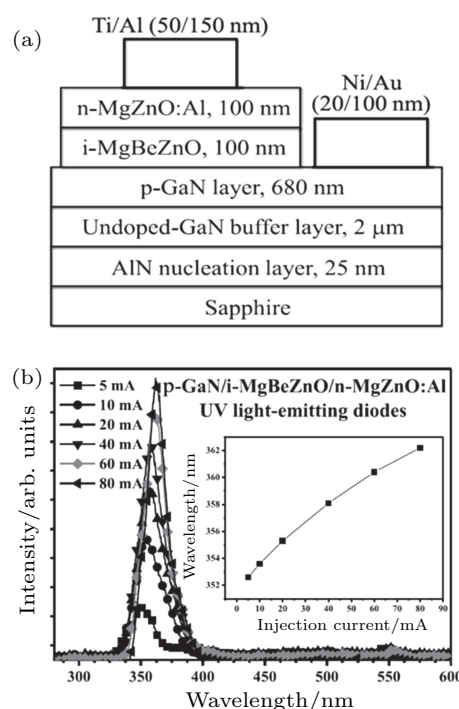


**Fig. 16.** (a) The schematic diagram of the  $\text{n-MgZnO:Al/i-Be}_{0.083}\text{Mg}_{0.047}\text{Zn}_{0.87}\text{O/p-GaN}$  heterostructured LED. (b) EL spectra of the UV LED injected with currents from 5 mA to 80 mA. The inset shows the emission peak wavelength *versus* injection current.<sup>[70]</sup>

#### 4. Conclusions

Alloying with MgO and BeO, the ZnO possesses the bandgap that can be modulated to cover the DUV region. In recent years, many efforts have been made to develop the ZnO-based DUV LEDs. However, the efficient p-type doping of ZnO is still an obstacle, and the p-type doping of MgZnO may be more challenging due to its wider bandgap. To avoid the obstacle of p-type doping of wide bandgap semiconductor, ZnO

based DUV LED has been fabricated by using the impact ionization process or high-energy electron beam as an excitation source. These results shown above reveal the prospect of ZnO-based DUV LEDs, but for the future applications, the performances of the devices still need further improving.

## References

- [1] Oto T, Banal R G, Kataoka K, Funato M and Kawakami Y 2010 *Nat. Photon.* **4** 645
- [2] Watanabe K, Taniguchi T, Niiyama T, Miya K and Taniguchi M 2009 *Nat. Photon.* **3** 591
- [3] Schubert E F and Cho J 2010 *Nat. Photon.* **4** 735
- [4] Adivarahan V, Heidari A, Zhang B, Fareed Q, Hwang S, Islam M and Khan A 2009 *Appl. Phys. Express* **2** 102101
- [5] Zhang Y T, Xia X C, Wu B, Shi Z F, Yang F, Yang X T, Zhang B L and Du G T 2014 *Chin. Phys. Lett.* **31** 058101
- [6] Taniyasu Y, Kasu M and Makimoto T 2006 *Nature* **441** 325
- [7] Zhong H M, Lu W, Sun Y and Li Z F 2007 *Chin. Phys. Lett.* **24** 2678
- [8] Aoyagi Y and Kurose N 2013 *Appl. Phys. Lett.* **102** 041114
- [9] Xia X C, Wang H, Zhao Y, Wang J, Zhao J Z, Shi Z F, Li X P, Liang H W, Zhang B L and Du G T 2011 *Chin. Phys. Lett.* **28** 108101
- [10] Hirayama H, Noguchi N, Yatabe T and Kamata N 2008 *Appl. Phys. Express* **1** 051101
- [11] Sang D D, Li H D, Chegn S H, Wang Q L, Yu Q and Yang Y Z 2012 *Appl. Phys. Lett.* **112** 036101
- [12] Wei B, Liu J Z, Zhang Y, Zhang J H, Peng H N, Fan H L, He Y B and Gao X C 2010 *Adv. Funct. Mater.* **20** 2448
- [13] Tan S, Egawa T, Luo X D, Sun L, Zhu Y H and Zhang J C 2016 *J. Phys. D: Appl. Phys.* **49** 125102
- [14] Reich C, Guttman M, Feneberg M, Wernicke T, Mehnke F, Kuhn C, Rass J, Laperrade M, Einfeldt S and Knauer A 2015 *Appl. Phys. Lett.* **107** 142101
- [15] Goh E S M, Yang H Y, Han Z J, Chen T P, Ostrikov K 2012 *Appl. Phys. Lett.* **101** 263506
- [16] Zhou S Q, Wu M F, Yao S D, Wang L and Jiang F Y 2006 *Chin. Phys. Lett.* **23** 1023
- [17] Wang Z J, Wang Z J, Li S C, Wang Z H, Lv Y M and Yuan J S 2004 *Chin. Phys. Lett.* **13** 750
- [18] Zhao F Q, Zhang M and Bai J H 2015 *Chin. Phys. B* **24** 097105
- [19] Ohtomo A, Kawasaki M, Koida T, Masubuchi K, Koinuma H, Sakurai Y, Yoshida Y, Yasuda T and Segawa Y 1998 *Appl. Phys. Lett.* **72** 2466
- [20] Ohtomo A, Tamura K, Kawasaki M, Makino T, Segawa Y, Tang Z K, Wong G K L, Matsumoto Y and Koinuma H 2000 *Appl. Phys. Lett.* **77** 2204
- [21] Gruber T, Kirchner C, Kling R, Reuss F, Waag A 2004 *Appl. Phys. Lett.* **84** 5359
- [22] Kim W J, Leem J H, Han M S, Park I W, Ryu Y R and Lee T S 2006 *J. Appl. Phys.* **99** 096104
- [23] Ryu Y, Lee T S, Lubguban J A, White H W, Kim B J, Park Y S and Youn C J 2006 *Appl. Phys. Lett.* **88** 241108
- [24] Su Y Q, Chen M M, Su L X, Zhu Y and Tang Z K 2016 *Chin. Phys. B* **25** 066106
- [25] Roessler D M and Walker W C 1967 *Phys. Rev.* **159** 733
- [26] Boguslawski P and Bernholc J 1997 *Phys. Rev. B* **56** 9496
- [27] Look D C, Clafflin B, Alivov Y I and Park S J 2004 *Phys. Status Solidi A* **201** 2203
- [28] Thomas M A and Cui J B 2010 *J. Phys. Chem. Lett.* **1** 1090
- [29] Shan C X, Liu J S, Lu Y J, Li B H, Ling F C and Shen D Z 2015 *Opt. Lett.* **40** 3041
- [30] Liu J S, Shan C X, Shen H, Li B H, Zhang Z Z, Liu L, Zhang L G and Shen D Z 2012 *Appl. Phys. Lett.* **101** 011106
- [31] Liu X Y, Shan C X, Jiao C, Wang S P, Zhao H F and Shen D Z 2014 *Opt. Lett.* **39** 422
- [32] Liu J S, Shan C X, Li B H, Zhang Z Z, Liu K W and Shen D Z 2013 *Opt. Lett.* **38** 2113
- [33] Echresh A, Chey C O, Shoushtari M Z, Nur O and Willander M 2015 *J. Lumin.* **160** 305
- [34] Zhu H, Shan C X, Li B H, Zhang J Y, Yao B, Zhang Z Z, Zhao D X, Shen D Z and Fan X W 2009 *J. Phys. Chem. C* **113** 2980
- [35] Chu S, Zhao S J, Xiong Z Q and Chu G 2011 *J. Nanosci. Nanotechnol.* **11** 8527
- [36] Walker L G and Pratt G W 1976 *J. Appl. Phys.* **47** 2129
- [37] Lagerstedt O, Monemar B and Gislason H 1978 *J. Appl. Phys.* **49** 2953
- [38] Thomas B W and Walsh D 1973 *Electron Lett.* **9** 362
- [39] Xu Y, Li Y P, Jin Y, Ma X Y and Yang D R 2013 *Acta Phys. Sin.* **62** 084207 (in Chinese)
- [40] Wang H T, Kang B S, Chen J J, Anderson T, Jang S and Ren F 2006 *Appl. Phys. Lett.* **88** 102107
- [41] Hwang D K, Oh M S, Lim J H, Choi Y S and Park S J 2007 *Appl. Phys. Lett.* **91** 121113
- [42] Minamim T, Tanigawa A, Yamanishi M and Kawamura T 1974 *Jpn. J. Appl. Phys.* **13** 1475
- [43] Chen P L, Ma X Y and Yang D R 2006 *Appl. Phys. Lett.* **89** 111112
- [44] Zhu H, Shan C X, Zhang J Y, Zhang Z Z, Li B H, Zhao D X, Yao B, Shen D Z, Fan X W, Tang Z K, Hou X and Choy K L 2010 *Adv. Mater.* **22** 1877
- [45] Zhu H, Shan C X, Li B H, Zhang Z Z, Shen D Z and Choy K L 2011 *J. Mater. Chem.* **21** 2848
- [46] Zhu H, Shan C X, Li B H, Zhang Z Z, Yao B and Shen D Z 2011 *Appl. Phys. Lett.* **99** 101110
- [47] Watanabe K, Taniguchi T and Kanda H 2004 *Nat. Mater.* **3** 404
- [48] Koizumi S, Watanabe K, Hasegawa M and Kanda H 2001 *Science* **292** 1899
- [49] Nakajima Y, Kojima A and Koshida N 2002 *Appl. Phys. Lett.* **81** 2472
- [50] Yoshiki N, Tetsuya U, Hajime T, Akira K, Bernard G and Nobuyoshi K 2004 *Jpn. J. Appl. Phys.* **43** 2076
- [51] Jiang W, Zhao S, Xu Z and Zhang F 2008 *Displays* **29** 432
- [52] Zhao S, Xu Z, Zhang F, Wang Y, Ji G and Xu X 2009 *J. Appl. Phys.* **106** 023513
- [53] Ni P N, Shan C X, Wang S P, Li B H, Zhang Z Z and Shen D Z 2012 *Opt. Lett.* **37** 15681
- [54] Ni P N, Shan C X, Li B H and Shen D Z 2014 *Appl. Phys. Lett.* **104** 032107
- [55] Xu T N, Wu H Z, Qiu D J and Chen N B 2003 *Chin. Phys. Lett.* **20** 1829
- [56] Khoshman J M, Ingram D C and Kordesch M E 2008 *Appl. Phys. Lett.* **92** 0919021
- [57] Wu C X, Lv Y M, Shen D Z, Wei Z P, Zhang Z Z, Li B H, Zhang J Y, Liu Y C and Fan X W 2005 *Chin. Phys. Lett.* **22** 2655
- [58] Chang Y S, Chien C T, Chen C W, Chu T Y, Chiang H H, Ku C H, Wu J J, Lin C S, Chen L C and K H Chen 2007 *J. Appl. Phys.* **101** 033502
- [59] Zhu Y, Chen M M, Su L X, Su Y Q, Ji X, Gui X C and Tang Z K 2014 *J. Alloys Compd.* **616** 505
- [60] Ryu Y R, Lee T S, Lubguban J A, Corman A B, White H W, Leem J H, Han M S, Park Y S, Youn C J and Kim W J 2006 *Appl. Phys. Lett.* **88** 052103
- [61] Ryu Y, Lee T S, Lubguban J A, White H W, Kim B J, Park Y S and Youn C J 2006 *Appl. Phys. Lett.* **88** 241108
- [62] Ryu Y, Lubguban J A, Lee T S, White H W, Jeong T S, Youn C J and Kim B J 2007 *Appl. Phys. Lett.* **90** 131115
- [63] Ganmukhi R, Calciati M, Goano M and Bellotti E 2012 *Semicond. Sci. Technol.* **27** 125015
- [64] Chen A, Zhu H, Wu Y, Chen M, Zhu Y, Gui X and Tang Z K 2016 *Adv. Funct. Mater.* **26** 3696
- [65] Furno E, Chiaria S, Penna M, Bellotti E and Goano M 2010 *J. Electron. Mater.* **39** 936
- [66] Panwar N, Liriano J and Katiyar R S 2011 *J. Alloys Compd.* **509** 1222
- [67] Su X, Si P, Hou Q, Kong X and Cheng W 2009 *Physica B* **404** 1794
- [68] Yang C, Li X M, Gao X D, Cao X, Yang R and Li Y Z 2010 *J. Cryst. Growth* **312** 978
- [69] Yang C, Li X M, Gu Y F, Yu W D, Gao X D and Zhang Y W 2008 *Appl. Phys. Lett.* **93** 112114
- [70] Lee H Y, Chang H Y, Lou L R and Lee C T 2008 *IEEE Photon. Technol. Lett.* **25** 1770